
Thin and Deep Gaussian Processes

Daniel Augusto de Souza*
University College London

Alexander Nikitin
Aalto University

ST John
Aalto University

Magnus Ross
University of Manchester

Mauricio A. Álvarez
University of Manchester

Marc Peter Deisenroth
University College London

João P. P. Gomes
Federal University of Ceará

Diego Mesquita
Getulio Vargas Foundation

César Lincoln C. Mattos
Federal University of Ceará

Abstract

Gaussian processes (GPs) can provide a principled approach to uncertainty quantification with easy-to-interpret kernel hyperparameters, such as the lengthscale, which controls the correlation distance of function values. However, selecting an appropriate kernel can be challenging. Deep GPs avoid manual kernel engineering by successively parameterizing kernels with GP layers, allowing them to learn low-dimensional embeddings of the inputs that explain the output data. Following the architecture of deep neural networks, the most common deep GPs warp the input space layer-by-layer but lose all the interpretability of shallow GPs. An alternative construction is to successively parameterize the lengthscale of a kernel, improving the interpretability but ultimately giving away the notion of learning lower-dimensional embeddings. Unfortunately, both methods are susceptible to particular pathologies which may hinder fitting and limit their interpretability. This work proposes a novel synthesis of both previous approaches: Thin and Deep GP (TDGP). Each TDGP layer defines locally linear transformations of the original input data maintaining the concept of latent embeddings while also retaining the interpretation of lengthscales of a kernel. Moreover, unlike the prior solutions, TDGP induces non-pathological manifolds that admit learning lower-dimensional representations. We show with theoretical and experimental results that i) TDGP is, unlike previous models, tailored to specifically discover lower-dimensional manifolds in the input data, ii) TDGP behaves well when increasing the number of layers, and iii) TDGP performs well in standard benchmark datasets.

1 Introduction

Gaussian processes (GPs) are probabilistic models whose nonparametric nature and interpretable hyperparameters make them appealing in many applications where uncertainty quantification and data efficiency matter, such as Bayesian optimization [11], spatiotemporal modeling [6], robotics and control [5]. The key modeling choice for a GP prior is its covariance or kernel function, which determines the class of functions it represents. However, due to finite data and a fixed-form kernel function, the GP may not inter- or extrapolate as desired. Stationary kernels, such as the commonly used squared exponential kernel and the Matérn family, assume the existence of a constant characteristic lengthscale, which makes them unsuitable for modeling non-stationary data.

To construct more expressive kernels, we can consider hierarchical GP models (deep GPs or DGP). The most common deep GP construction is a functional composition of GP layers with standard

*Contact: daniel.souza.21@ucl.ac.uk.

stationary kernels that results in a non-stationary non-Gaussian process [3, 23]; for clarity, we will refer to this model type as compositional DGPs (CDGPs). However, CDGPs can show pathological behavior, where adding layers leads to a *loss* of representational ability [9, 7]. Alternatively, it is also possible to extend “shallow” GPs by making the kernel lengthscales a function of the input [19], resulting in the deeply non-stationary GP [DNSGP, 22]. Although this covariance function approach to DGPs does not degenerate with more layers, care must be taken to guarantee a positive semi-definite kernel matrix. Moreover, the induced space is not a proper inner-product space [18], which hinders the learning of useful manifolds.

In this paper, we address the shortcomings of previous DGPs paradigms by retaining the flexibility provided by learning hierarchical lengthscale fields while also enabling manifold learning. Instead of pursuing neural networks to enhance standard GPs [1, 26], which may lead to overfitting [17], we retain the nonparametric formulation by using additional GPs to model a linear projection of each input onto a latent manifold. The key insight of our approach is that such projections are input-dependent and tailored towards more interpretable lower-dimensional manifolds with corresponding length-scale fields. The resulting Thin and Deep GP² (TDGP) avoids the pitfalls of other DGP constructions while maintaining its hierarchical composition and modeling capacity beyond shallow GPs.

Our contributions are three-fold:

1. We propose TDGP, a new hierarchical architecture for DGPs that is highly interpretable and does not degenerate as the number of layers increases. Notably, TDGP is the only deep architecture that induces both a lengthscale field and data embeddings.
2. We prove that TDGPs and compositional DGPs are the limits of a more general DGP construction. Thus, we establish a new perspective on standard CDGPs while reaping the benefits of inducing a lengthscale field
3. We demonstrate that TDGPs perform as well as or better than previous approaches. Our experiments also show that TDGP leans towards inducing low-dimensional embeddings.

2 Background

Gaussian processes (GPs) are distributions over functions and fully characterized by a mean function m and a kernel (covariance function) k [20]. If a function f is GP distributed, we write $f \sim \text{GP}(m, k)$. If not stated otherwise, we assume that the prior mean function is 0 everywhere, i.e., $m(\cdot) \equiv 0$. Typically, the kernel possesses a few interpretable hyper-parameters, such as lengthscales or signal variances, estimated by the standard maximization of the marginal likelihood [20].

The squared exponential (SE) kernel is arguably the most commonly used covariance function in the GP literature and, in its most general form [25], it can be written as

$$k_{\text{SE}}(\mathbf{a}, \mathbf{b}) = \sigma^2 \exp\left[-\frac{1}{2}(\mathbf{a} - \mathbf{b})^\top \mathbf{\Delta}^{-1}(\mathbf{a} - \mathbf{b})\right], \quad (1)$$

where $\mathbf{a}, \mathbf{b} \in \mathbb{R}^D$, the constant $\sigma^2 > 0$ defines the signal variance, and $\mathbf{\Delta} \in \mathbb{R}^{D \times D}$ is a lengthscale matrix. Notably, the SE kernel is *stationary*, i.e., $k_{\text{SE}}(\mathbf{a} + \mathbf{c}, \mathbf{b} + \mathbf{c}) = k_{\text{SE}}(\mathbf{a}, \mathbf{b})$ for any $\mathbf{c} \in \mathbb{R}^D$. Furthermore, when the lengthscale matrix $\mathbf{\Delta} = \lambda^2 \mathbf{I}$, the kernel is *isotropic*, meaning that it can be written as a function $\pi_{\text{SE}}(d^2)$ of the squared distance $d^2 = \|\mathbf{a} - \mathbf{b}\|_2^2$. For more details on the significance of the lengthscale parameter, we refer the reader to Appendix A.

Stationary kernels enforce invariances, which may not always be desirable. However, stationary kernels can be used as building blocks to derive broader families of kernels (including *non-stationary* kernels), either by composing them with deformation functions or through mixtures of lengthscales.

Deformation kernels result from applying a deformation function $\tau : \mathbb{R}^D \rightarrow \mathbb{R}^Q$ to \mathbf{a} and \mathbf{b} before feeding them to a stationary kernel k in \mathbb{R}^Q . Thus, a deformation kernel k_τ follows

$$k_\tau(\mathbf{a}, \mathbf{b}) = k(\tau(\mathbf{a}), \tau(\mathbf{b})). \quad (2)$$

For a linear transformation $\tau(\mathbf{x}) = \mathbf{W}\mathbf{x}$, we can interpret k_τ as a stationary kernel with lengthscale matrix $\mathbf{\Delta} = [\mathbf{W}^\top \mathbf{W}]^{-1}$. However, for more intricate $\tau(\cdot)$, interpreting or analyzing k_τ can be very challenging. For instance, this is the case for deep kernel learning [DKL, 26] models, in which $\tau(\cdot)$ is an arbitrary neural network.

²“Thin” refers to the graph-theoretical girth of the graphical model of our proposed DGP construction.

Compositional deep GPs [CDGPs, 3] also rely on deformation kernels, but they use a GP prior to model $\tau(\cdot)$. The kernel of the $\tau(\cdot)$ process can also (recursively) be considered to be a deformation kernel, thereby extending DGPs to arbitrary depths. However, stacking GP layers reduces the interpretability of DGPs, and their non-injective nature makes them susceptible to pathologies [9].

Lengthscale mixture kernels [19] are a generalization of the process of convolving stationary kernels with different lengthscales from Higdon et al. [14]. For arbitrary isotropic kernels k , i.e., $k(\mathbf{a}, \mathbf{b}) = \pi_k(\|\mathbf{a} - \mathbf{b}\|_2^2)$, Paciorek and Schervish [19] construct a non-stationary k_{lmx} as a function of a field of lengthscale matrices $\Delta : \mathbb{R}^D \rightarrow \mathbb{R}^{D \times D}$, such that

$$k_{\text{lmx}}(\mathbf{a}, \mathbf{b}) = |\Delta(\mathbf{a})|^{\frac{1}{4}} |\Delta(\mathbf{b})|^{\frac{1}{4}} |(\Delta(\mathbf{a}) + \Delta(\mathbf{b}))/2|^{-\frac{1}{2}} \pi_k(\delta), \quad (3)$$

where $\delta = 2(\mathbf{a} - \mathbf{b})^\top (\Delta(\mathbf{a}) + \Delta(\mathbf{b}))^{-1} (\mathbf{a} - \mathbf{b})$. The explicit lengthscale field Δ makes this model more interpretable than general deformation kernels. However, Paciorek [18] notes that $\delta(\mathbf{a}, \mathbf{b})$ may violate the triangle inequality and therefore does not induce a manifold over the input space. This departure from the properties of stationary kernels is due to the matrix inside the quadratic form being a function of both \mathbf{a} and \mathbf{b} . Another caveat is that the scale of k_{lmx} is also controlled by a pre-factor term that depends on Δ , allowing for unintended effects (such as unwanted long-range correlations), especially in rapidly varying lengthscale fields.

Deeply non-stationary GPs [DNSGPs, 7, 22] use the lengthscale mixture kernel and parameterize the function $\Delta(\mathbf{x})$ with a warped GP prior to obtain a deep GP model. Similar to CDGPs, this model can be extended in depth [22, 7] by considering the kernel of $\Delta(\mathbf{x})$ to be non-stationary with its lengthscales stemming from another GP. A practical issue in these models is guaranteeing that $\Delta(\mathbf{x})$ is positive semi-definite. Therefore, in practice, $\Delta(\mathbf{x})$ is usually restricted to be diagonal.

3 Thin and deep GPs (TDGPs)

As discussed in the previous section, deep GP constructions follow naturally from hierarchical extensions of a base kernel. Therefore, we arrange the presentation of TDGPs in three parts. First, we propose a *kernel* that admits interpretations both in terms of its lengthscale and of its induced manifold. Second, we use this kernel to build a novel type of deep GP *model* (TDGP). Third, we describe how to carry out *inference* for TDGPs. Finally, we discuss *limitations* of our approach.

Kernel. We address the drawbacks of the approaches based on deformation and lengthscale mixture kernels — i.e., the lack of interpretability and failure to induce a manifold, respectively — by proposing a synthesis of both methods, retaining their positives whilst mitigating some of their issues. Starting from the discussion in Section 2, a squared exponential kernel with lengthscale matrix $[\mathbf{W}^\top \mathbf{W}]^{-1}$ corresponds to a deformation of an isotropic kernel:

$$\begin{aligned} k_{\text{SE}}(\mathbf{a}, \mathbf{b}) &= \pi_{\text{SE}}((\mathbf{a} - \mathbf{b})^\top \mathbf{W}^\top \mathbf{W} (\mathbf{a} - \mathbf{b})) \\ &= \pi_{\text{SE}}((\mathbf{W}\mathbf{a} - \mathbf{W}\mathbf{b})^\top (\mathbf{W}\mathbf{a} - \mathbf{W}\mathbf{b})) \\ &= \pi_{\text{SE}}(\|\mathbf{W}\mathbf{a} - \mathbf{W}\mathbf{b}\|_2^2). \end{aligned} \quad (4)$$

Therefore, this is the same as applying a linear deformation $\tau(\mathbf{x}) = \mathbf{W}\mathbf{x}$.

We propose extending this to a non-linear transformation that is locally linear by letting \mathbf{W} vary as a function of that input, so $\tau(\mathbf{x}) = \mathbf{W}(\mathbf{x})\mathbf{x}$. This results in the TDGP kernel:

$$\begin{aligned} k_{\text{TDGP}}(\mathbf{a}, \mathbf{b}) &= \pi_{\text{SE}}(\|\mathbf{W}(\mathbf{a})\mathbf{a} - \mathbf{W}(\mathbf{b})\mathbf{b}\|_2^2) \\ &= \pi_{\text{SE}}((\mathbf{W}(\mathbf{a})\mathbf{a} - \mathbf{W}(\mathbf{b})\mathbf{b})^\top (\mathbf{W}(\mathbf{a})\mathbf{a} - \mathbf{W}(\mathbf{b})\mathbf{b})). \end{aligned} \quad (5)$$

Equation (5) cannot be written as a Mahalanobis distance like in Eq. (4), but in the neighborhood of \mathbf{x} , $[\mathbf{W}^\top(\mathbf{x})\mathbf{W}(\mathbf{x})]^{-1}$ is a lengthscale matrix, thus allowing k_{TDGP} to be implicitly parametrized by a lengthscale field just like the lengthscale mixture kernels of Paciorek and Schervish [19]. Hence, it allows for better interpretability than the deformation kernels considered in compositional DGPs.

However, unlike the lengthscale mixture approach of Eq. (3), our kernel in Eq. (5) does not introduce an input-dependent pre-factor, thereby avoiding pathologies when the lengthscale varies rapidly. Moreover, since the distance induced by the quadratic form obeys the triangle inequality, it induces a manifold in the input space. Hence, it addresses the two issues of lengthscale mixture kernels.

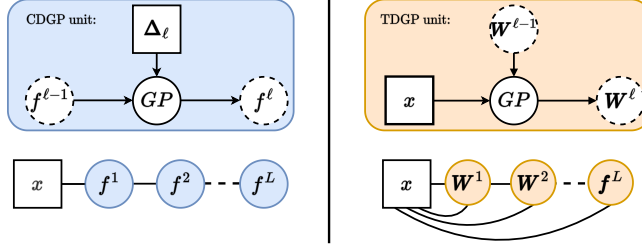


Figure 1: Graphical models for a CDGP (left) and TDGP (right) with L layers. The colored boxes represent the architecture of a single layer; dashed nodes represent where layers connect. CDGP directly composes functions, whereas TDGP builds a hierarchy of input-dependent lengthscales fields.

Model. In an analogous manner to the compositional DGP and DNSGP, we present how to use this kernel to build a hierarchical GP model. Our L -layers deep model is described as follows:

$$p(f^L(\cdot) | \mathbf{h}^{L-1}(\cdot)) = \text{GP}(f | 0, \pi_k(\|\mathbf{h}^{L-1}(\mathbf{a}) - \mathbf{h}^{L-1}(\mathbf{b})\|)), \quad (6)$$

where

$$\mathbf{h}^\ell(\mathbf{x}) = \mathbf{W}^\ell(\mathbf{h}^{\ell-1}(\mathbf{x}))\mathbf{x}, \quad \mathbf{h}^0(\mathbf{x}) = \mathbf{x}, \quad (7)$$

$$p(\mathbf{W}^\ell(\cdot)) = \prod_{d=1}^D \prod_{q=1}^Q \text{GP}(w_{qd}^\ell | \mu_w^\ell, k_w^\ell). \quad (8)$$

Therefore, this model can be extended arbitrarily by deforming the kernel of the entries of \mathbf{W}^ℓ with another locally linear transformation with its own matrix $\mathbf{W}^{\ell-1}$.

Figure 1 compares the graphical model of TDGP and compositional DGP. We notice that TDGP learns hierarchical input-dependent lengthscales fields, instead of a straight composition of processes. We call this model **Thin and deep GP** (TDGP) by the fact that our graphical model always has cycles of bounded length due to the connection of every hidden layer with the inputs \mathbf{X} . Therefore, it has finite girth, in contrast to the unbounded girth of the compositional DGP graphical model. Importantly, however, TDGP are related to CDGPs as both can be seen as locally affine deformations of the input space (proof in Appendix B).

Theorem 3.1 (Relationship between TDGP and CDGP). *Any L -layer CDGP prior over a function $f(\mathbf{x}) = h^L(\mathbf{h}^{L-1}(\dots \mathbf{h}^1(\mathbf{x}) \dots))$ is a special case of a generalized TDGP prior with equal depth defined over the augmented input space $\tilde{\mathbf{x}} = [\mathbf{x}, 1]^\top$. Since linear deformations $\tilde{\mathbf{W}}\tilde{\mathbf{x}}$ in the augmented space correspond to affine transformations $\mathbf{W}\mathbf{x} + \mathbf{d}$ in the original space, the special case of the CDGP model corresponds to a TDGP where the prior variance of \mathbf{W}^ℓ approaches zero.*

Unlike DNSGP, which makes the positive semi-definite matrix Δ a function and requires the use of warped GP priors, our hidden layers \mathbf{W} are arbitrary matrices that admit a regular Gaussian prior. By placing zero-mean priors on the entries of \mathbf{W} , we encourage the MLE estimate to maximally reduce the latent dimensionality of \mathbf{h} . This is because the latent dimensionality becomes linked to the number of rows with non-zero variance in the prior, e.g., if the prior kernel variance i -th row of \mathbf{W}^ℓ tends to zero, the posterior over that row is highly concentrated at zero, eliminating the i -th latent dimension. In a compositional DGP, this inductive bias also corresponds to a zero-mean prior in the hidden layers. However, as discussed by Duvenaud et al. [9], and reproduced in Fig. 2, this choice introduces a pathology that makes the derivatives of the process almost zero.

Inference. To estimate the posterior distributions and the hyperparameters of our model, we perform variational inference (VI). We introduce inducing points \mathbf{u} for the last-layer GP $f(\cdot)$ and inducing points \mathbf{V} for the $W(\cdot)$ processes. Similar to how VI methods for DGPs [3] were based on the non-deep GPLVM model [24], our method builds upon VI for the hyperparameters of square exponential kernels in shallow GPs as discussed by Damianou et al. [4]. However, we replace the Gaussian prior $p(\mathbf{W})$ with a GP prior $p(\mathbf{W}(\cdot))$. For instance, the variational distribution for a two-layer TDGP is:

$$q(\mathbf{f}, \mathbf{W}, \mathbf{u}, \mathbf{V}) = p(\mathbf{f} | \mathbf{u}) \mathcal{N}(\mathbf{u} | \check{\boldsymbol{\mu}}_u, \check{\boldsymbol{\Sigma}}_u) \prod_{d=1}^D \prod_{q=1}^Q p(w_{qd} | v_{qd}) \mathcal{N}(v_{qd} | \check{\boldsymbol{\mu}}_{v_{qd}}, \check{\boldsymbol{\Sigma}}_{v_{qd}}), \quad (9)$$

where for the final layer the parameters $\check{\mu}_u, \check{\Sigma}_u$ are not estimated but replaced with their closed-form optimal solutions. Appendix C contains a derivation of the ELBO and more details.

Limitations. For large numbers of layers, our VI scheme for TDGP may become computationally intensive. By stacking additional hidden layers $\mathbf{W}(\mathbf{x})$, we add $D \times Q$ GPs into the model; consequently, the number of variational parameters increases, which can slow down optimization. More specifically, inference uses $\mathcal{O}(L \times D \times Q \times m^2)$ parameters and takes time $\mathcal{O}(L \times D \times Q \times (m^2 + m^2n))$ to compute the ELBO. Additional details on runtime as a function of data size and width can be found in the Appendix E. Furthermore, without the addition of a bias to the input data \mathbf{x} , TDGP performs locally linear transformations $\mathbf{W}(\mathbf{x})\mathbf{x}$, meaning that the neighborhood of $\mathbf{x} = \mathbf{0}$ is kept unchanged for each layer.

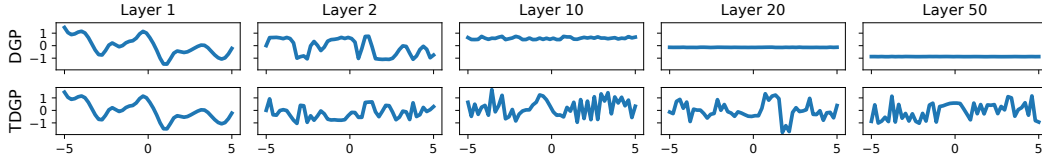


Figure 2: Samples from a CDGP prior (top row) and a TDGP prior (bottom row), both with zero mean. Each column represents the number of layers, where one layer corresponds to a regular shallow GP. When the number of layers increases, CDGP samples quickly become flat, i.e. the prior distribution no longer supports ‘interesting’ functions. Notably, this pathology does not occur with TDGP.

4 Experiments

To assess whether TDGP accurately captures non-smooth behavior and has competitive results with other GP models, we performed a regression experiment on a synthetic dataset with input-dependent linear projections and another experiment in varied empirical datasets. In this section, we examine the two-layer TDGP against a two-layer CDGP, two-layer DNSGP, DKL, and the shallow sparse GP (SGP). These models are evaluated on average negative log-predictive density (NLPD) and mean relative absolute error (MRAE). All metrics are “the lower, the better”. Importantly, throughout the experiments, we also emphasize (i) the interpretability of our model compared to the prior art and (ii) TDGP’s inductive bias towards learning low-dimensional embeddings. In all experiments, inputs and targets are normalized so that the training set has zero mean and unit variance. Appendix D contains more details of architecture, training, and initialization. We implemented the experiments in Python using GPflow [10], GPflux [8], and Keras [2]. Code is available as supplementary material at <https://github.com/spectraldani/thindeepgps>.

4.1 Synthetic experiment

Data. To assess our intuition that TDGP leans towards inducing low-dimensional manifolds, we show how well TDGP and competitors can fit a composite function $f = g \circ h$, with $g : \mathbb{R} \rightarrow \mathbb{R}$ and $h : \mathbb{R}^2 \rightarrow \mathbb{R}$ are non-linear functions. In this context, h acts as a “funnel” inducing a 1D manifold. For more details on f and how we sample from the input space, we refer the reader to the appendix.

Results. Figure 3 shows the posterior mean of TDGP and competing methods for our synthetic dataset. Note TDGP accurately fits the target function (leftmost panel), while the other methods fail to capture the shape of 2/3 maxima regions. Consequently, Table 1 shows that TDGP performs significantly better in both in terms of NLPD and MRAE in the test data.

Examining the latent space. TDGP outperformed competitors in predictive performance, but how do their latent spaces compare? To further understand the nuances that distinguish each model, Fig. 4 plots their respective latent spaces and lengthscale fields — along with the true latent space induced by h as a baseline. While TDGP induces both a latent space and a lengthscale field, it is important to highlight that the same does not hold for CDGP and DNSGP. Thus, Fig. 4 does not show a latent space for DNSGP or a lengthscale field for CDGP. Notably, TDGP’s latent space perfectly captures

Table 1: Results for the synthetic data. TDGP significantly outperforms baselines.

	NLPD	MRAE
SGP	-1.49	0.11
DKL	36.82	0.21
CDGP	-1.28	0.12
DNSGP	-1.46	0.12
TDGP	-3.57	0.00

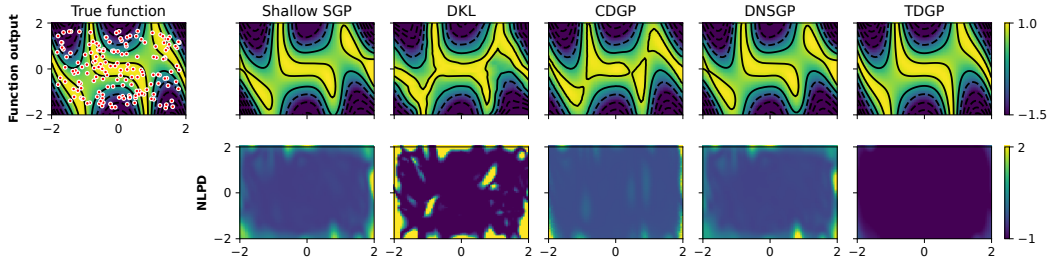


Figure 3: Synthetic 2D dataset with one latent dimension. The leftmost plot shows the true function and the location of the training data as red dots. The remaining plots show the mean predictions and NLPD of each method. TDGP presents the best fit for the true function, as observed by the mean and NLPD plots.

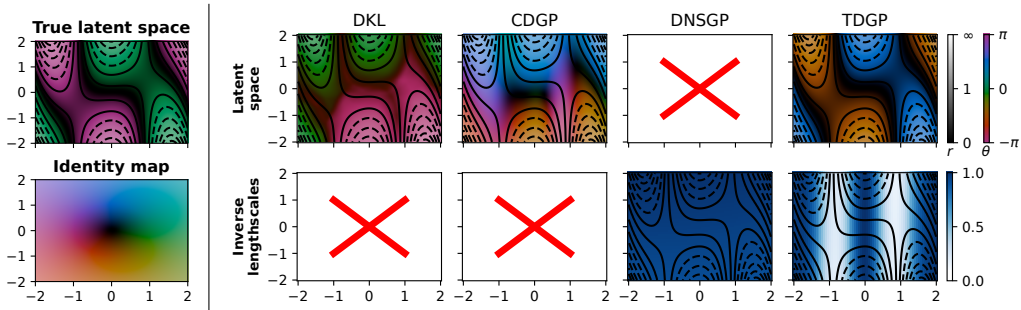


Figure 4: Synthetic dataset: true latent space (left), latent spaces learned by each model (top-right), and their inverse lengthscales (bottom-right). Models that do not induce a latent space or a lengthscale field are marked in **red crosses**. Note that TDGP is the only model that allows both interpretations. Furthermore, TDGP’s latent space perfectly captures the shape of the ground truth.

the shape of h , while DKL and CDGP fail to do so. Analyzing the lengthscales, we conclude that TDGP successfully learns a non-stationary kernel, unlike DNSGP.

Finally, Fig. 5 shows that TDGP learns to give much higher importance to one of its latent dimensions, supporting our intuition that TDGPs lean towards learning low-dimensional manifolds. While the shallow GP and CDGP also weigh one dimension higher than the other, this discrepancy is less accentuated. It is worth mentioning that measuring the relevance of latent dimensions depends on the architecture we evaluate. For DGPs and DKL, we can use the inverses of the output layer’s kernel lengthscales. Naturally, the same rationale applies to shallow GPs. For TDGP, the analogous variable is the kernel variance of each hidden layer’s row, since the larger this value is, the more distant from zero the values of that row are. Overall, these results suggest that TDGP leans towards learning sparser representations than its competitors.

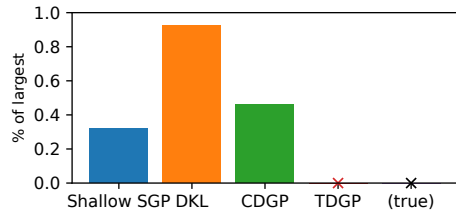


Figure 5: Synthetic dataset: what is the *effective* dimensionality of the inferred latent space? A dimension’s relevance is given by its inverse lengthscales; we plot the relative relevance of the least relevant compared to the largest. Only TDGP matches the one-dimensionality of the true latent space.

4.2 Bathymetry case study

Data. As a case-study, we also apply TDGP to the bathymetry dataset GEBCO. This dataset contains a global terrain model (elevation data) for ocean and land. We selected an especially challenging subset of the data (see the appendix for details) covering the Andes mountain range, ocean, and land as an example of a non-stationary task. We subsample 1,000 points from this region and compare the methods via five-fold cross-validation.

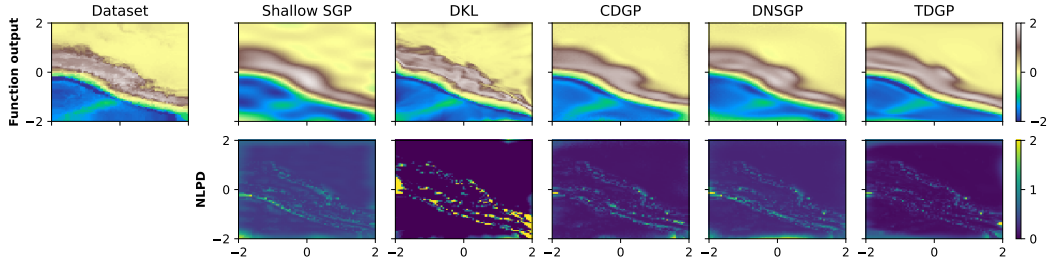


Figure 6: Results for GEBCO bathymetry dataset. The leftmost plot shows the dataset, while the remaining plots show the mean predictions and NLPD of each method. Note how, despite having the best mean posteriors, DKL has an overfitting problem, as shown in the NLPD. TDGP is the most balanced, especially when capturing the transitions between ocean/mountains/plains.

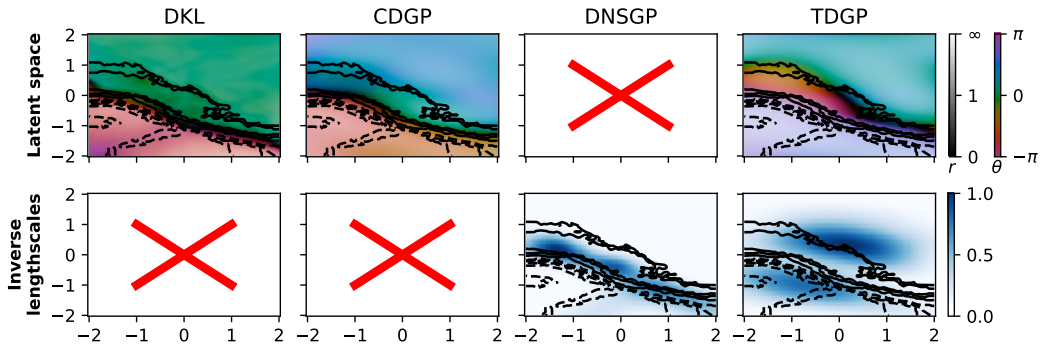


Figure 7: GEBCO dataset: visualization of the latent spaces learned by each model (top) and their inverse lengthscales fields (bottom). Models that do not induce a latent space or a lengthscale field are marked in **red crosses**. TDGP is the only model that allows both interpretations. For expert users, the lengthscale field is the only one on which informative priors can be put.

Results. The NLPD and MRAE results are listed in Table 2, where we observed our method to be slightly better than others. However, more importantly, this dataset can be thoroughly examined and interpreted. Figure 8 shows correlation plots for a point located on the lower slope of the Andes. We observe more sensible correlations for TDGP and CDGP compared to other methods — the correlation is high in the locations across the slope. This plot also highlights a recurring problem with DNSGP: Despite a high inverse lengthscales barrier in the Andes, there is still a correlation between the slope of the mountain and the sea level. Additionally, Fig. 7 shows the domain coloring of learned latent spaces and the sum of the eigenvalues of the lengthscales fields. Once again, we note that only TDGP can be analyzed in both ways. This is an advantage in settings where expert priors on the smoothness exist, as these can be placed directly in the lengthscales field instead of the less accessible latent space mapping. As expected, methods that learn the lengthscales field place high inverse lengthscales values around the mountain range and low values in the smooth oceans and plains.

Table 2: Performance of each model on the GEBCO dataset (avg±std). Lower is better.

	NLPD	MRAE
SGP	-0.13 ± 0.09	1.19 ± 0.63
DKL	3.85 ± 0.92	0.59 ± 0.31
CDGP	-0.44 ± 0.12	0.83 ± 0.56
DNSGP	-0.31 ± 0.12	1.12 ± 0.75
TDGP	-0.53 ± 0.10	0.66 ± 0.43

4.3 Benchmark datasets

Data. We also compare the methods in four well-known regression datasets from the UCI repository. To assess each model fairly, we adopt a ten-fold separation of the datasets into training and testing.

Results. Figure 9 shows the average NLPD for each method in the UCI datasets along with their respective standard deviations. TDGP performs either on par with other methods or outperforms them. Figure 10 also shows the relative relevance of each method’s latent dimensions. Similarly to what we observed in the synthetic experiments, TDGP’s inductive bias leads to a sharp split

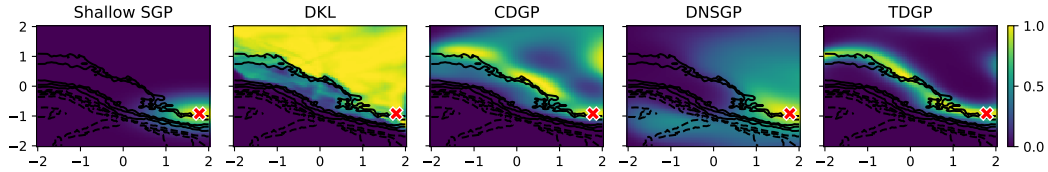


Figure 8: Correlation plots on GEBCO dataset for a datapoint marked \star (1.7, -0.9), which is located close to mountains. We observe better interpretability with TDGP (the zone of high correlation coincides with mountains) compared to DNSGP (high correlation extends into the sea and plains).

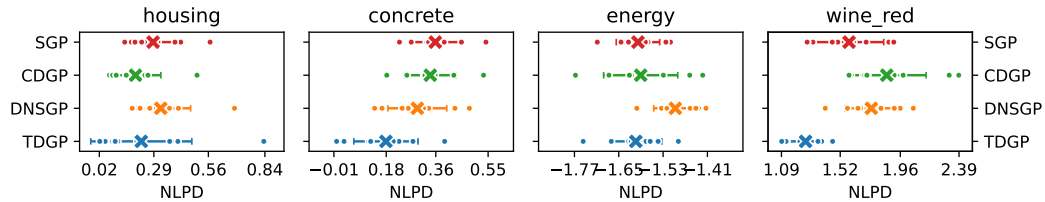


Figure 9: Benchmark datasets: test NLPD (lower is better) of each model for 10 folds. Each dot represents the result of a fold. The cross and bar represent the mean and standard deviation across all folds. TDGP is as good or better than the compared models.

between relevant and irrelevant dimensions, especially compared to the prior art. Even for the cases with close generalization errors, TDGP shows better interpretability and bias towards learning lower dimensional representations.

5 Related work

Expressive non-stationary GPs can be constructed in a variety of ways. We give a brief overview of some contributions available in the literature below.

Convolution of RBF and scale mixture kernels. Non-stationary covariance learning can be done by convolving two RBF kernels with different lengthscales. This well-studied approach was later extended to arbitrary kernels by Paciorek and Schervish [19]. Gibbs [12] introduced this formu-

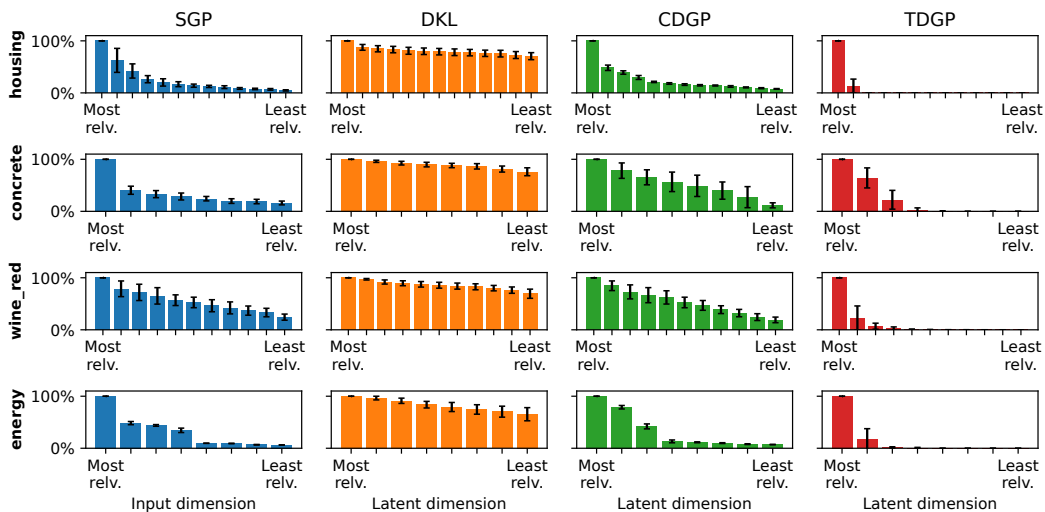


Figure 10: Benchmark datasets: comparison of the relevances of the latent dimensions identified by each model (mean and 1σ interval). TDGP consistently identifies low-dimensional latent spaces (most dimensions are irrelevant).

lation, representing the lengthscale as the sum of squares of an arbitrary function applied to each covariance input. Later, Higdon et al. [14] introduced this approach in the spatial context, varying the focus points of the ellipse representing the 2×2 lengthscale matrix of an RBF covariance with independent GPs, which constitutes a two-layer DGP in 2D. Heinonen et al. [13] introduced a method to jointly vary the covariance amplitude and lengthscale, and the observation noise over the domain, using Hamiltonian Monte Carlo for inference. As discussed in Section 2, all these methods inherit the limitations of their kernel, i.e. issues with the pre-factor and violation of the triangle inequality, which hinders manifold learning.

Compositional deep GPs. Compositional DGPs [15, 3] construct priors over complex functions by repeatedly applying a sequence of non-parametric transformations to the input, with each transformation being represented by a GP with a stationary covariance. One of the the most significant issues with CDGPs is that, unlike neural networks which compose linear functions through non-linear scalar activations, every latent layer is a non-linear function. Therefore, several authors have suggested improvements to DGPs by adding skip connections that directly concatenate the hidden layer with the input space [9] or the use of linear mean functions [16, 23] for improved performance and capability. CDGP research also explores improvements in inference, such as the use of mini-batching and more efficient approximations to intractable integrals [23], and the inclusion of auxiliary latent variables to allow for more flexible posteriors [21]. Since TDGP is based on deformation kernels and is related to CDGPs, we believe it can leverage many of these advances in inference, which is left to future investigations.

Deep kernel learning. An alternative to CDGPs is to use layers of parametric transformations to learn arbitrarily complex kernels. Deep kernel learning [1, 26] parameterizes such transformations with a deterministic neural network. Since these deep kernels have many parameters and are not constructed in a Bayesian way, they are prone to overfitting and miscalibrated uncertainties, and can perform poorly in practice [17]. Nevertheless, by using Bayesian injective warping functions that are well-suited for spatial applications, Zammit-Mangion et al. [27] were able to achieve good results in low-dimensional datasets.

6 Conclusion

This work presented Thin and Deep GP (TDGP), a new hierarchical architecture for DGPs. TDGP can recover non-stationary functions through a locally linear deformation of stationary kernels. Importantly, this construction allows us to interpret TDGP in terms of the latent embeddings and the lengthscale field it induces. Additionally, while TDGP shares a connection with CDGP, our prior does not concentrate on "flat" samples when the number of layers increases — as is the case with CDGP. Furthermore, our experiments show that TDGP performs as well as or better than the prior art. Moreover, TDGP has a robust inductive bias toward learning low-dimensional embeddings, which is instrumental for better interpretability.

That being said, we expect TDGP will be especially useful for geospatial modeling in cases where we are modeling non-stationary functions and when we have expert knowledge on how this function should vary over space/time, which could be inserted as priors over the locally linear transformations. We also believe that recent improvements in inference available in the literature could greatly enhance the expressivity and ease of training of TDGP.

Acknowledgments

This work was supported in part by the CONFAP-CNPq-THE UK Academies program (grant UKA-00160-00003.01.00/19). Diego Mesquita was supported by the Silicon Valley Community Foundation (SVCF) through the Ripple impact fund, the Fundação de Amparo à Pesquisa do Estado do Rio de Janeiro (FAPERJ) through the *Jovem Cientista do Nosso Estado* program, and the Fundação de Amparo à Pesquisa do Estado de São Paulo (FAPESP) through the grant 2023/00815-6.

References

- [1] Roberto Calandra, Jan Peters, Carl Edward Rasmussen, and Marc Peter Deisenroth. “Manifold Gaussian processes for regression”. In: *International Joint Conference on Neural Networks (IJCNN)*. 2016.
- [2] François Chollet. *Keras*. <https://keras.io>. 2015.
- [3] Andreas C. Damianou and Neil D. Lawrence. “Deep Gaussian processes”. In: *Artificial Intelligence and Statistics (AISTATS)*. 2013.
- [4] Andreas C. Damianou, Michalis K. Titsias, and Neil D. Lawrence. “Variational inference for latent variables and uncertain inputs in Gaussian processes”. In: *Journal of Machine Learning Research (JMLR)* 17 (2016).
- [5] Marc Peter Deisenroth and Carl Edward Rasmussen. “PILCO: A Model-Based and Data-Efficient Approach to Policy Search”. In: *International Conference on Machine Learning (ICML)*. 2011.
- [6] Peter J. Diggle and Paulo J. Ribeiro. “Gaussian models for geostatistical data”. In: *Model-based Geostatistics*. Springer New York, 2007, pp. 46–78.
- [7] Matthew M. Dunlop, Mark A. Girolami, Andrew M. Stuart, and Aretha L. Teckentrup. “How deep are deep Gaussian processes?” In: *Journal of Machine Learning Research (JMLR)* 19 (2018).
- [8] Vincent Dutordoir, Hugh Salimbeni, Eric Hambro, John McLeod, Felix Leibfried, Artem Artemev, Mark van der Wilk, Marc Peter Deisenroth, James Hensman, and S. T. John. “GPflux: A library for Deep Gaussian Processes”. In: (2021).
- [9] David Duvenaud, Oren Rippel, Ryan Adams, and Zoubin Ghahramani. “Avoiding pathologies in very deep networks”. In: *Artificial Intelligence and Statistics (AISTATS)*. 2014.
- [10] Alexander G. de G. Matthews, Mark van der Wilk, Tom Nickson, Keisuke Fujii, Alexis Boukouvalas, Pablo León-Villagrà, Zoubin Ghahramani, and James Hensman. “GPflow: A Gaussian Process Library using TensorFlow”. In: *Journal of Machine Learning Research (JMLR)* 18 (2017).
- [11] Roman Garnett. *Bayesian Optimization*. Cambridge University Press, 2023.
- [12] Mark N. Gibbs. “Bayesian Gaussian processes for regression and classification”. PhD thesis. University of Cambridge, 1997.
- [13] Markus Heinonen, Henrik Mannerström, Juho Rousu, Samuel Kaski, and Harri Lähdesmäki. “Non-Stationary Gaussian Process Regression with Hamiltonian Monte Carlo”. In: *Artificial Intelligence and Statistics (AISTATS)*. 2016.
- [14] Dave Higdon, Jenise Swall, and John Kern. “Non-Stationary Spatial Modeling”. In: 6. 1999.
- [15] Neil D. Lawrence and Andrew J. Moore. “Hierarchical Gaussian process latent variable models”. In: *international Conference on Machine learning (ICML)*. 2007.
- [16] Miguel Lázaro-Gredilla. “Bayesian Warped Gaussian Processes”. In: *Advances in Neural Information Processing Systems (NeurIPS)*. 2012.
- [17] Sebastian W. Ober, Carl Edward Rasmussen, and Mark van der Wilk. “The promises and pitfalls of deep kernel learning”. In: *Uncertainty in Artificial Intelligence (UAI)*. 2021.
- [18] Christopher J. Paciorek. “Nonstationary Gaussian Processes for Regression and Spatial Modelling”. PhD thesis. Carnegie Mellon University, 2003.
- [19] Christopher J. Paciorek and Mark J. Schervish. “Nonstationary Covariance Functions for Gaussian Process Regression”. In: *Advances in Neural Information Processing Systems (NeurIPS)*. 2003.
- [20] Carl Edward Rasmussen and Christopher K. I. Williams. *Gaussian Processes for Machine Learning*. MIT Press, 2006.
- [21] Hugh Salimbeni. “Deep Gaussian Processes: Advances in Models and Inference”. PhD thesis. Imperial College London, 2019.
- [22] Hugh Salimbeni and Marc Peter Deisenroth. “Deeply non-stationary Gaussian processes”. In: *2nd Workshop on Bayesian Deep Learning (NeurIPS)*. 2017.
- [23] Hugh Salimbeni and Marc Peter Deisenroth. “Doubly Stochastic Variational Inference for Deep Gaussian Processes”. In: *Advances in Neural Information Processing Systems (NeurIPS)*. 2017.

- [24] Michalis K. Titsias and Neil D. Lawrence. “Bayesian Gaussian Process Latent Variable Model”. In: *Artificial Intelligence and Statistics (AISTATS)*. 2010.
- [25] Michalis K. Titsias and Miguel Lázaro-Gredilla. “Variational Inference for Mahalanobis Distance Metrics in Gaussian Process Regression”. In: *Advances in Neural Information Processing Systems (NeurIPS)*. 2013.
- [26] Andrew Gordon Wilson, Zhiting Hu, Ruslan Salakhutdinov, and Eric P. Xing. “Deep Kernel Learning”. In: *Artificial Intelligence and Statistics (AISTATS)*. 2016.
- [27] Andrew Zammit-Mangion, Tin Lok James Ng, Quan Vu, and Maurizio Filippone. “Deep Compositional Spatial Models”. In: *Journal of the American Statistical Association* 117.540 (2022).

A Interpretation of lengthscale parameters

First, we start with the stationary case. There exist stationary kernels k which can be represented as:

$$k(\mathbf{a}, \mathbf{b}) = \pi_k((\mathbf{a} - \mathbf{b})^\top \mathbf{\Delta}^{-1}(\mathbf{a} - \mathbf{b})), \quad (10)$$

for a given scalar function π_k and lengthscale parameter $\mathbf{\Delta}$. In this case, the lengthscale controls the spatial variation of the Gaussian process with that kernel. More concretely, in the 1D case, using scalar lengthscale $\mathbf{\Delta} = \ell^2$ and the squared exponential kernel:

$$k_{\text{SE}}(a, b) = \exp \left[-\frac{1}{2} \frac{(a - b)^2}{\ell^2} \right], \quad (11)$$

we have that the corresponding marginals for $f \sim \text{GP}(0(\cdot), k_{\text{SE}})$ are:

$$f(x) \sim \mathcal{N}(0, 1), \quad (12)$$

$$\frac{d}{dx} f(x) \sim \mathcal{N}\left(0, \frac{1}{\ell^2}\right). \quad (13)$$

So the lengthscale parameter directly controls the amplitude of the gradient's variance.

In general, non-stationary kernels do not have a corresponding concept, which attention is given to kernels that, in the neighborhood of a point \mathbf{x} , can be expressed in terms of a local lengthscale matrix $\mathbf{\Delta}(\mathbf{x})$. The lengthscale mixture kernels k_{lmx} described in Section 2 and our proposed kernel from Section 3, k_{TDGP} both have this local lengthscale property.

Again, assuming inputs are 1D and the base kernel is squared exponential, both kernels are:

$$k_{\text{lmx}}(a, b) = \ell(a)^{\frac{2}{4}} \ell(b)^{\frac{2}{4}} \left[\frac{\ell(a)^2 + \ell(b)^2}{2} \right]^{-\frac{1}{2}} \exp \left[-\frac{1}{2} \frac{(a - b)^2}{\frac{\ell(a)^2 + \ell(b)^2}{2}} \right],$$

$$k_{\text{TDGP}}(a, b) = \exp \left[-\frac{1}{2} \left(\frac{a}{\ell(a)} - \frac{b}{\ell(b)} \right)^2 \right].$$

And in terms of derivatives:

$$\frac{d}{dx} f_{\text{lmx}}(x) \sim \mathcal{N}\left(0, \frac{2 + \frac{d}{dx} \ell(x)^2}{2\ell(x)^2}\right), \quad (14)$$

$$\frac{d}{dx} f_{\text{TDGP}}(x) \sim \mathcal{N}\left(0, \frac{(\ell(x) - x \frac{d}{dx} \ell(x))^2}{\ell(x)^4}\right). \quad (15)$$

Both kernels generalize Eq. (13) and, as expected, recover the stationary case when $\frac{d}{dx} \ell(x) = 0$.

Note that the domain of the lengthscale function $\ell(x)$ is always the domain of the function f , meaning that as we consider deeper models, the lengthscale function is always a function of the original domain. This is unlike the general compositional case, e.g. $f(g(h(x)))$, where the domain of each individual function is the image of the previous function. Moreover, the relationship with the lengthscale parameter and derivative of the output function remains clear.

B TDGP and CDGP are limits of a generalized DGP

Theorem 3.1. Any L -layer CDGP prior over a function $f(\mathbf{x}) = h^L(\mathbf{h}^{L-1}(\dots \mathbf{h}^1(\mathbf{x}) \dots))$ is a special case of a TDGP prior with equal depth defined over the augmented input-space $\tilde{\mathbf{x}} = [\mathbf{x}, 1]^\top$. Since linear deformations $\tilde{\mathbf{W}}\tilde{\mathbf{x}}$ in the augmented space correspond to affine transformations $\mathbf{W}\mathbf{x} + \mathbf{d}$ in the original space, the special case of the CDGP model corresponds to a TDGP where the prior variance of the \mathbf{W}^ℓ approaches zero.

Proof. First, we append a bias to the input data: $\tilde{\mathbf{x}} = [\mathbf{x} \ 1]^\top \in \mathbb{R}^{D+1}$. Therefore, the hidden-layer matrices need to be expanded so that $\tilde{\mathbf{W}}(\tilde{\mathbf{h}}) \in \mathbb{R}^{(Q+1) \times (D+1)}$. Then, choose the following form for

$\tilde{\mathbf{W}}$:

$$\tilde{\mathbf{W}}(\tilde{\mathbf{h}}) = \begin{bmatrix} \mathbf{W}(\mathbf{h}) & \mathbf{d}(\mathbf{h}) \\ \mathbf{0}_{1 \times Q} & 1 \end{bmatrix}, \quad (16)$$

where,

$$\mathbf{W}(\cdot) \in \mathbb{R}^{Q \times D} \sim \prod_{q=1}^Q \prod_{d=1}^D \text{GP}(w_{qd}(\cdot) \mid 0(\cdot), k_{w_{qd}}), \quad (17)$$

$$\mathbf{d}(\mathbf{x}) \in \mathbb{R}^Q \sim \prod_{q=1}^Q \text{GP}(d_q(\cdot) \mid \mu_{d_q}, k_{d_q}). \quad (18)$$

Note that $\tilde{\mathbf{W}}(\cdot)$ still follows the TDGP prior because all of its entries are either GP distributed or limits of GP priors, like in the case of the lower row where the Dirac delta distributions can be obtained by taking the limit of the kernel variance parameter σ^2 to zero.

Then, the ℓ -th latent space of this model is:

$$\tilde{\mathbf{h}}^\ell = \tilde{\mathbf{W}}(\tilde{\mathbf{h}}^{\ell-1}) \tilde{\mathbf{x}} \quad (19)$$

$$= \begin{bmatrix} \mathbf{W}(\mathbf{h}^{\ell-1}) & \mathbf{d}(\mathbf{h}^{\ell-1}) \\ \mathbf{0}_{1 \times Q} & 1 \end{bmatrix} \begin{bmatrix} \mathbf{x} \\ 1 \end{bmatrix} \quad (20)$$

$$= \begin{bmatrix} \mathbf{W}(\mathbf{h}^{\ell-1}) \mathbf{x} + \mathbf{d}(\mathbf{h}^{\ell-1}) \cdot 1 \\ 0 \cdot \mathbf{x} + 1 \end{bmatrix} \quad (21)$$

$$= [\mathbf{W}(\mathbf{h}^{\ell-1}) \mathbf{x} + \mathbf{d}(\mathbf{h}^{\ell-1}) \quad 1]^\top \quad (22)$$

$$= [\mathbf{h}^\ell \quad 1]^\top. \quad (23)$$

By ignoring the bias dimension, we get a latent space \mathbf{h} that includes a multiplicative component $\mathbf{W}(\cdot)$ and an additive component $\mathbf{d}(\cdot)$. If the prior variance of $\mathbf{W}(\cdot)$ goes to zero, which is controlled by the kernel variance hyperparameter, then $\mathbf{W}(\cdot) \rightarrow \mathbf{0}$, resulting in only the additive component remaining:

$$\mathbf{h}^\ell = \mathbf{d}(\mathbf{h}^{\ell-1}), \quad (24)$$

which recovers the traditional compositional deep GP. \square

Note that if $\mu_{d_q}(\cdot)$ is also a zero function, then, if the prior variance of $\mathbf{d}(\cdot)$ tends to zero, then $\mathbf{d}(\cdot) \rightarrow \mathbf{0}$, meaning that $\mathbf{h} = \mathbf{W}(\mathbf{h}^{\ell-1}) \mathbf{x}$, which recovers the original TDGP model.

C Variational inference

First, the prior L -layer TDGP model as defined in Section 3 is

$$p(f^L(\cdot) \mid \mathbf{h}^{L-1}(\cdot)) = \text{GP}(f \mid 0, \pi_k(\|\mathbf{h}^{L-1}(\mathbf{a}) - \mathbf{h}^{L-1}(\mathbf{b})\|)), \quad (25)$$

where

$$\mathbf{h}^\ell(\mathbf{x}) = \mathbf{W}^\ell(\mathbf{h}^{\ell-1}(\mathbf{x})) \mathbf{x}, \quad \mathbf{h}^0(\mathbf{x}) = \mathbf{x}, \quad (26)$$

$$p(\mathbf{W}^\ell(\cdot) \mid \mathbf{h}^{\ell-1}(\cdot)) = \prod_{d=1}^D \prod_{q=1}^{Q_\ell} \text{GP}(w_{qd}^\ell \mid \mu_{w_{qd}^\ell}, \pi_{k_{w_{qd}^\ell}}^\ell(\|\mathbf{h}^{\ell-1}(\mathbf{a}) - \mathbf{h}^{\ell-1}(\mathbf{b})\|)). \quad (27)$$

We now introduce inducing points for each GP layer in this process. The last-layer process has inducing points \mathbf{u}^L and each hidden layer has inducing points \mathbf{V}^ℓ defined as follows:

$$\mathbf{u}^L = f^L(\mathbf{Z}^L), \quad \mathbf{V}^\ell = \mathbf{W}^\ell(\mathbf{Z}^\ell), \quad (28)$$

where we also introduce L sets of pseudo-inputs $\{\mathbf{Z}^\ell \in \mathbb{R}^{m_\ell \times Q_\ell} \mid \ell \in [1, L]\}$. Finally, we define the variational distribution as follows:

$$q(f^L, \mathbf{u}, \{\mathbf{W}^\ell, \mathbf{V}^\ell\}) = p(f(\cdot) \mid \mathbf{u}^L) q(\mathbf{u}^L) \prod_{\ell=1}^{L-1} \prod_{d=1}^D \prod_{q=1}^{Q_\ell} p(\mathbf{w}_{qd}^\ell(\cdot) \mid \mathbf{v}_{qd}^\ell) q(\mathbf{v}_{qd}^\ell), \quad (29)$$

where

$$q(\mathbf{u}^L) = \mathcal{N}(\mathbf{u}^L \mid \check{\boldsymbol{\mu}}_u^L, \check{\boldsymbol{\Sigma}}_u^L), \quad q(\mathbf{v}_{qd}^\ell) = \mathcal{N}(\mathbf{v}_{qd}^\ell \mid \check{\boldsymbol{\mu}}_{v_{qd}}^\ell, \check{\boldsymbol{\Sigma}}_{v_{qd}}^\ell). \quad (30)$$

The main simplification of this ELBO is to make each layer conditionally independent of each other when conditioned on the set of inducing variables.

C.1 Simplification for efficiency

In order to simplify this model, first, we will make each row of $\mathbf{W}^\ell(\cdot)$ share the same kernel and kernel hyperparameters, this means that the variational posterior covariance of \mathbf{V}^ℓ are also shared, i.e., $\check{\boldsymbol{\Sigma}}_{v_{qd}}^\ell = \check{\boldsymbol{\Sigma}}_{v_{qd'}}^\ell$ for every d and d' , so we will represent this as $\check{\boldsymbol{\Sigma}}_{v_q}^\ell$. Secondly, to compute some expectations in closed form, following Titsias and Lázaro-Gredilla [6], we will consider all kernels to be squared exponential kernels. So that $\pi_k(r) = \sigma_f^2 \exp[-0.5r^2]$ and $\pi_{k_{w_{qd}}}^\ell(r) = \sigma_q^2 \exp[-0.5r^2]$.

And then, the prior model and variational distributions become:

$$\begin{aligned} p(f^L(\cdot) \mid \mathbf{h}^{L-1}(\cdot)) &= \text{GP}(f \mid 0, \sigma_f^2 \exp[-0.5\|\mathbf{h}^{L-1}(\mathbf{a}) - \mathbf{h}^{L-1}(\mathbf{b})\|^2]), \\ p(w_{qd}^\ell(\cdot) \mid \mathbf{h}^{\ell-1}(\cdot)) &= \text{GP}(w_{qd}^\ell \mid \mu_{w_{qd}}^\ell, \sigma_{w_q}^2 \exp[-0.5\|\mathbf{h}^{\ell-1}(\mathbf{a}) - \mathbf{h}^{\ell-1}(\mathbf{b})\|^2]), \\ q(\mathbf{u}^L) &= \mathcal{N}(\mathbf{u}^L \mid \check{\boldsymbol{\mu}}_u^L, \check{\boldsymbol{\Sigma}}_u^L), \\ q(\mathbf{v}_{qd}^\ell) &= \mathcal{N}(\mathbf{v}_{qd}^\ell \mid \check{\boldsymbol{\mu}}_{v_{qd}}^\ell, \check{\boldsymbol{\Sigma}}_{v_q}^\ell). \end{aligned}$$

C.2 Two-layer model

Finally, we will work on the model with a single hidden layer $\mathbf{W}(\cdot)$ and one output layer $f(\cdot)$. Again, the prior model is simplified to:

$$p(f(\cdot) \mid \mathbf{h}(\cdot)) = \text{GP}(f \mid 0, \sigma_f^2 \exp[-0.5\|\mathbf{h}(\mathbf{a}) - \mathbf{h}(\mathbf{b})\|^2]), \quad (31)$$

where

$$p(\mathbf{W}(\cdot) \mid \mathbf{h}(\cdot)) = \prod_{d=1}^D \prod_{q=1}^Q \text{GP}\left(w_{qd} \mid \mu_{w_{qd}}^\ell, \sigma_{w_q}^2 \exp\left[-0.5\left\|\frac{\mathbf{a}}{l} - \frac{\mathbf{b}}{l}\right\|^2\right]\right), \quad (32)$$

$$\mathbf{h}(\mathbf{x}) = \mathbf{W}(\mathbf{x}) \mathbf{x}. \quad (33)$$

Accordingly, the variational distribution becomes:

$$q(\mathbf{u}) = \mathcal{N}(\mathbf{u} \mid \check{\boldsymbol{\mu}}_u, \check{\boldsymbol{\Sigma}}_u), \quad q(\mathbf{v}_{qd}) = \mathcal{N}(\mathbf{v}_{qd} \mid \check{\boldsymbol{\mu}}_{v_{qd}}, \check{\boldsymbol{\Sigma}}_{v_q}). \quad (34)$$

C.3 Evidence lower bound (ELBO)

As in Titsias and Lázaro-Gredilla [6] and Titsias [4], we will consider the marginals of $f(\cdot)$ and $\mathbf{W}(\cdot)$ evaluated at the training data (\mathbf{X}, \mathbf{y}) , $\mathbf{f} \in \mathbb{R}^n = \mathbf{f}(\mathbf{X})$ and $\mathbf{W} \in \mathbb{R}^{n \times Q \times D} = \mathbf{W}(\mathbf{X})$. Following the definition of the ELBO, we have the following lower bound on the evidence:

$$p(\mathbf{y}) = \langle p(\mathbf{y} \mid \mathbf{f}) \rangle_{p(\mathbf{f}, \mathbf{W})} \quad (35)$$

$$\geq \boxed{\langle \log p(\mathbf{y} \mid \mathbf{f}) \rangle_{q(\mathbf{f}, \mathbf{u}, \mathbf{W}, \mathbf{v})} - \text{KL}(q(\mathbf{u}) \parallel p(\mathbf{u}))} - \sum_{d=1}^D \sum_{q=1}^Q \text{KL}(q(\mathbf{v}_{dq}) \parallel p(\mathbf{v}_{dq})). \quad (36)$$

Given our simplifying assumptions from before and choice of variational distribution, the terms inside the **blue box** have the same form as the ELBO of Titsias and Lázaro-Gredilla [6], therefore the value of the **blue box** with optimal $q(\mathbf{u})$ is:

$$\begin{aligned} \blacksquare &= -\frac{1}{2\sigma^2} (\mathbf{y}^\top \mathbf{y} + \psi_0 - \text{Tr}[\mathbf{K}_u^{-1} \boldsymbol{\Psi}_2]) - \frac{n}{2} \ln(2\pi\sigma^2) \\ &\quad + \frac{1}{2\sigma^2} \mathbf{y}^\top \boldsymbol{\Psi}_1 \boldsymbol{\Sigma}^{-1} \boldsymbol{\Psi}_1^\top \mathbf{y} + \frac{m_u}{2} \ln(\sigma^2) - \frac{1}{2} \ln|\boldsymbol{\Sigma}| + \frac{1}{2} \ln|\mathbf{K}_u|, \end{aligned} \quad (37)$$

where the Ψ -statistics [5, 6] are defined as:

$$\psi_0 = \langle \text{Tr } \mathbf{K}_f \rangle_{q(\mathbf{W}, \mathbf{V})} = n\sigma_f^2, \quad \Psi_1 = \langle \mathbf{K}_{fu} \rangle_{q(\mathbf{W}, \mathbf{V})}, \quad \Psi_2 = \langle \mathbf{K}_{fu}^\top \mathbf{K}_{fu} \rangle_{q(\mathbf{W}, \mathbf{V})}, \quad (38)$$

and the optimal $q(\mathbf{u})$ is:

$$q(\mathbf{u}) = \mathcal{N}\left(\mathbf{u} \mid \mathbf{K}_u [\sigma^2 \mathbf{K}_u + \Psi_2]^{-1} \Psi_1^\top \mathbf{y}, \sigma^2 \mathbf{K}_u (\sigma^2 \mathbf{K}_u + \Psi_2)^{-1} \mathbf{K}_u\right) \quad (39)$$

C.4 Computing the Ψ -statistics

The trick for computing the Ψ statistics is to show that each entry of the matrices only depends on a specific $\mathbf{W}(\mathbf{x}_i)$ and can be expressed as a product in the rows q , therefore allowing us to marginalize $q(\mathbf{W}, \mathbf{V})$ to $\prod_{d=1}^D q(\mathbf{w}_{iqd}, \mathbf{v}_{iqd})$. So, starting with Ψ_1 :

$$[\Psi_1]_{ij} = \langle [\mathbf{K}_{fu}]_{ij} \rangle_{q(\mathbf{W}, \mathbf{V})} \quad (40)$$

$$= \left\langle \sigma_f \exp \left[-\frac{1}{2} (\mathbf{W}_i \mathbf{x}_i - \mathbf{z}_j^{(1)}) (\mathbf{W}_i \mathbf{x}_i - \mathbf{z}_j^{(1)})^\top \right] \right\rangle_{q(\mathbf{W})}, \quad (41)$$

so we can marginalize $q(\mathbf{W})$,

$$= \left\langle \sigma_f \exp \left[-\frac{1}{2} (\mathbf{W}_i \mathbf{x}_i - \mathbf{z}_j^{(1)}) (\mathbf{W}_i \mathbf{x}_i - \mathbf{z}_j^{(1)})^\top \right] \right\rangle_{q(\mathbf{W}_i)} \quad (42)$$

$$= \left\langle \sigma_f \exp \left[-\frac{1}{2} \sum_{q=1}^Q (\mathbf{w}_{iq}^\top \mathbf{x}_i - z_{jq}^{(1)})^2 \right] \right\rangle_{q(\mathbf{W}_i)} \quad (43)$$

$$= \sigma_f \prod_{q=1}^Q \left\langle \exp \left[-\frac{1}{2} (\mathbf{w}_{iq}^\top \mathbf{x}_i - z_{jq}^{(1)})^2 \right] \right\rangle_{q(\mathbf{w}_{iq})}. \quad (44)$$

This is the same situation as in Appendix B.1 of [6], so:

$$[\Psi_1]_{ij} = \sigma_f \prod_{q=1}^Q \left(\mathbf{x}_i^\top \tilde{\Sigma}_q \mathbf{x}_i + 1 \right)^{-\frac{1}{2}} \exp \left[-\frac{1}{2} \frac{(\tilde{\boldsymbol{\mu}}_{iq}^\top \mathbf{x}_i - z_{jq}^{(1)})^2}{\left(\mathbf{x}_i^\top \tilde{\Sigma}_q \mathbf{x}_i + 1 \right)} \right], \quad (45)$$

where $\tilde{\boldsymbol{\mu}}_{iq}$ and $\tilde{\Sigma}_q$ are the mean and covariance of $\prod_{d=1}^D q(\mathbf{w}_{iqd})$. Now, for Ψ_2 :

$$[\Psi_2]_{jk} = \left\langle [\mathbf{K}_{fu}^\top \mathbf{K}_{fu}]_{jk} \right\rangle_{q(\mathbf{W}, \mathbf{V})} \quad (46)$$

$$= \left\langle \sum_{i=1}^n [\mathbf{K}_{fu}]_{ij} [\mathbf{K}_{fu}]_{ik} \right\rangle_{q(\mathbf{W}, \mathbf{V})} \quad (47)$$

$$= \sum_{i=1}^n \left\langle [\mathbf{K}_{fu}]_{ij} [\mathbf{K}_{fu}]_{ik} \right\rangle_{q(\mathbf{W}_i)}. \quad (48)$$

Again, following [6]:

$$\begin{aligned} [\Psi_2]_{jk} &= \sigma_f^2 \exp \left[-\frac{1}{4} \sum_{q=1}^Q (z_{jq}^{(1)} - z_{kq}^{(1)})^2 \right] \\ &\quad \times \sum_{i=1}^n \prod_{q=1}^Q \left(2\mathbf{x}_i^\top \tilde{\Sigma}_q \mathbf{x}_i + 1 \right)^{-\frac{1}{2}} \exp \left[-\frac{(\tilde{\boldsymbol{\mu}}_{iq}^\top \mathbf{x}_i - \tilde{z}_q)^2}{2\mathbf{x}_i^\top \tilde{\Sigma}_q \mathbf{x}_i + 1} \right], \end{aligned} \quad (49)$$

where $\tilde{z}_q = \frac{z_{jq}^{(1)} + z_{kq}^{(1)}}{2}$.

D Details on experiments

Setting. For each experiment, we performed cross-validation (five folds for bathymetry and 10 folds for UCI). We compare the generalization error using MRAE and compare the uncertainty quantification using NLPD. We used the Adam optimizer, and the following schedule (we varied Adam step size and likelihood variance):

- For 500 epochs: step size 0.1, and likelihood variance fixed to 0.01,
- For 1500 epochs: step size 0.01, and likelihood variance fixed to 0.01,
- For 5000 epochs: step size 0.001, and likelihood variance is trainable.

Architecture. The architectural details of each model are:

SGPR 50 inducing points for the output process and an ARD-squared exponential kernel. Inference is done by using the optimal $q(\mathbf{u})$ as described by Titsias [4].

DKL 50 inducing points for the output process and an ARD-squared exponential kernel. For the deep kernel, we use an MLP with architecture $[D, 500, 50, D]$, where D is the dimension of the inputs and a final BatchNorm layer. All hidden-layer activations are ReLU. Inference is done by using the optimal $q(\mathbf{u})$ as described by Titsias [4].

CDGP 50 inducing points for the output process and 25 for the latent space process. All layers use an ARD-squared exponential kernel. The dimension of the hidden layer is set to D . We use doubly stochastic inference [3] with whitened variables, i.e. we reparametrize \mathbf{u} as $\mathbf{K}_u^{-\frac{1}{2}}\mathbf{u}$.

DNSGP 50 inducing points for the output process and 25 for the lengthscale matrix space process. All layers use an ARD-squared exponential kernel and the lengthscale matrix process is set to be diagonal with warping function $\exp(\mathbf{h} + s)$, where s is a learnable scalar. We use doubly stochastic inference [3] with whitened variables, i.e. we reparametrize \mathbf{u} as $\mathbf{K}_u^{-\frac{1}{2}}\mathbf{u}$.

TDGP 50 inducing points for the output process and 25 for the inverse lengthscale matrix space process. The size of the inverse lengthscale matrix \mathbf{W} is set to $Q \times D$, where $Q = D$ and each row q of shares the same kernel. Our variational posterior distribution in $q(\mathbf{V})$ is set to mean-field where $q(\mathbf{V}) = \prod_{i=1}^n \prod_{q=1}^Q \prod_{d=1}^D q(v_{iqd})$.

D.1 Synthetic experiment

Data. We generated a synthetic dataset by definition a composite function $f = g \circ h$, with $g : \mathbb{R} \rightarrow \mathbb{R}$ and $h : \mathbb{R}^2 \rightarrow \mathbb{R}$ are non-linear functions. In this context, h acts as a “funnel” inducing a 1D manifold. These functions are defined as:

$$h(\mathbf{x}) = 2x_0 \sin(x_0\pi) + 2 \cos(x_0\pi) \tag{50}$$

$$g(z) = \frac{\sin(z)}{z} - z^2. \tag{51}$$

Then, we uniformly sample \mathbf{x} in the interval $[-1, 1] \times [-1, 1]$ and split 50/50 for train and validation.

D.2 Bathymetry case study

Data. The selected subset of GEBCO data covers the Andes mountain range, ocean, and land as an example of a non-stationary task (longitude in the range from -80 to -60 , and latitude in the range from -20 to -10). We randomly subsampled 1000 data points.

Computational resources. Running all the models took 2.5 hours using an NVIDIA A100 GPU. More fine-grained time measurements are presented in Table 3.

Table 3: Training and evaluation time (seconds) in GEBCO dataset (avg±std). Lower is better.

	Train	Evaluation
SGP	23.4 ± 1.5	0.03 ± 0.01
DKL	384.6 ± 8.5	0.76 ± 1.28
CDGP	570.8 ± 0.6	0.14 ± 0.17
DNSGP	596.4 ± 29.8	0.06 ± 0.01
TDGP	126.7 ± 0.8	0.12

Table 4: Training time (seconds) for the benchmark datasets (avg±std). Lower is better.

	housing	concrete	energy	wine_red
SGP	41.4 ± 0.2	41.0 ± 0.7	41.5 ± 1.2	42.6 ± 2.0
DKL	379.1 ± 3.7	379.0 ± 3.5	376.7 ± 2.3	386.1 ± 13.4
CDGP	601.5 ± 9.4	592.1 ± 4.1	592.9 ± 3.5	615.4 ± 23.5
DNSGP	668.0 ± 75.9	621.8 ± 2.2	620.8 ± 1.9	650.8 ± 24.0
TDGP	572.4 ± 12.4	563.7 ± 1.8	484.3 ± 1.4	928.6 ± 42.1

D.3 Benchmark datasets

Data. We used a subset of datasets from the UCI repository: housing³, concrete⁴, wine-red⁵, and energy datasets.⁶

Housing dataset has 506 samples with 13 features; concrete dataset has 1030 samples with 8 features; wine-red has 1599 samples with 11 features; energy dataset has 768 samples with 8 features.

Computational resources. Training all models in all datasets for ten folds took 25.55 hours using an NVIDIA TITAN RTX GPU. Per dataset time measurements are presented in Table 4

E Computational and test performance as a function of width

In the experiments of Section 4, the width of the hidden layer Q for TDGP was always set to match the dimension of the input D . As seen in Fig. 10, after optimization of the hyperparameters, the effective width of the layer for all datasets was always much smaller than D . Therefore, it is reasonable to expect that a wider model wouldn't increase the model's performance.

Nevertheless, we conduct an additional experiment to explore the performance penalty of increasing Q up to D in terms of computational resources and test accuracy. In the chosen housing dataset, Fig. 10 shows that $Q \approx 2 < D$ is the effective width of an optimized network. Therefore, we re-run this experiment with values of Q ranging from 1 to D as shown in Fig. 11.

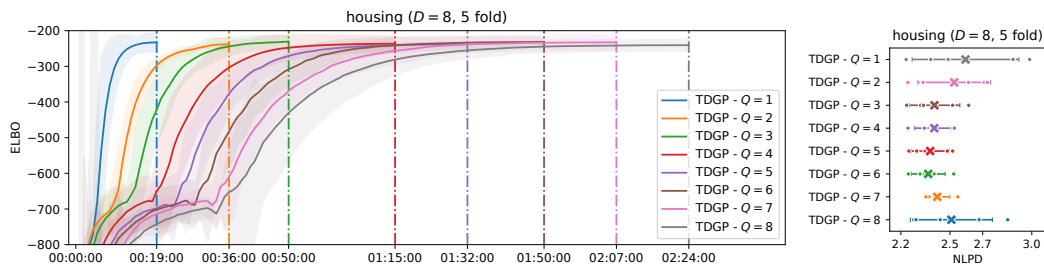


Figure 11: Training curves (left) and test metrics (right) for the housing dataset with a variable width Q

³<https://archive.ics.uci.edu/ml/machine-learning-databases/housing/>

⁴<https://archive.ics.uci.edu/ml/datasets/Concrete+Compressive+Strength>

⁵<https://archive.ics.uci.edu/ml/datasets/Wine+Quality, red variant>

⁶<https://archive.ics.uci.edu/ml/datasets/energy+efficiency>

As discussed, we observe a linear increase in training time as the model’s width increases. In terms of predictive performance, the best widths are 3 to 6; in theory, we wouldn’t expect a performance drop above a certain minimum width, as the effective width is a trained variable, however, as stated in our limitation, we expected the increased number of variables to optimize to add more complexity to the optimization landscape and, therefore, increase the difficulty in finding the best set of hyperparameters.

F Expressivity of the prior with increasing depth

The TDGP model as defined in Section 3 places a zero-mean prior on all the layers. This is in contrast with the standard CDGP model, which as shown in Duvenaud et al. [1], suffers prior collapse under this assumption. Figure 2 shows this effect by plotting different samples from CDGP and TDGP priors with zero mean as the model depth increases. Nonetheless, as shown in Salimbeni and Deisenroth [2], another way to visualize this pathology is to plot samples of the covariance matrix as the number of layers increase.

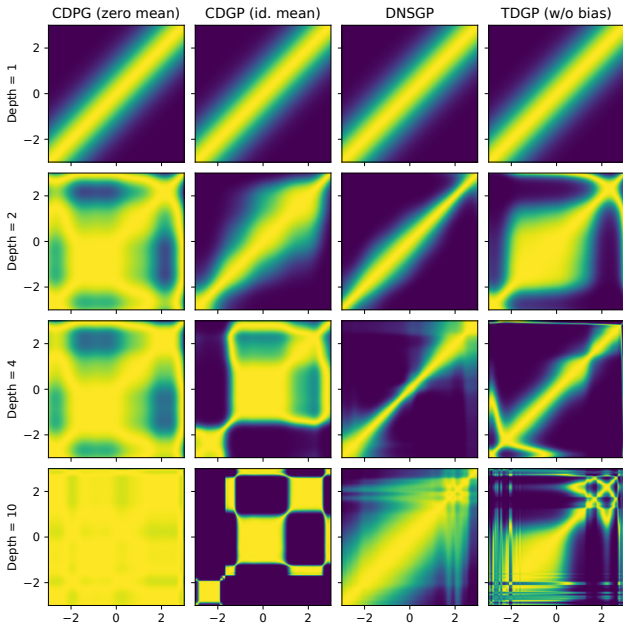


Figure 12: Samples from the prior covariance matrix for different layers and models

As shown in Fig. 12, as the model depth increases, the covariance matrix of CDGP with zero mean eventually saturates, i.e. all points are high correlated, which leads to the flat priors shown in Fig. 2. We can also see that, as discussed in Salimbeni and Deisenroth [3], changing the zero-mean prior to one with an linear mean function fixes this pathology, as well as using a zero-mean DNSGP or a zero-mean TDGP model. This is further evidence that our model

G Societal and broader impact

Gaussian processes are popular methods for spatiotemporal modeling in, e.g., climatology, geoscience, public health, and ecology. This work proposes TDGP, a novel formulation for deep GPs that preserves the performance of compositional deep GPs while significantly improving their interpretability. We believe the inherent interpretability of TDGP priors will make it easier for applied researchers to encode their subjective knowledge, consequently improving the data efficiency of their models and reducing predictive uncertainties. Additionally, we do not foresee any negative societal impact stemming directly from this work.

References

- [1] David Duvenaud, Oren Rippel, Ryan Adams, and Zoubin Ghahramani. “Avoiding pathologies in very deep networks”. In: *Artificial Intelligence and Statistics (AISTATS)*. 2014.
- [2] Hugh Salimbeni and Marc Peter Deisenroth. “Deeply non-stationary Gaussian processes”. In: *2nd Workshop on Bayesian Deep Learning (NeurIPS)*. 2017.
- [3] Hugh Salimbeni and Marc Peter Deisenroth. “Doubly Stochastic Variational Inference for Deep Gaussian Processes”. In: *Advances in Neural Information Processing Systems (NeurIPS)*. 2017.
- [4] Michalis K. Titsias. “Variational Learning of Inducing Variables in Sparse Gaussian Processes”. In: *Artificial Intelligence and Statistics (AISTATS)*. 2009.
- [5] Michalis K. Titsias and Neil D. Lawrence. “Bayesian Gaussian Process Latent Variable Model”. In: *Artificial Intelligence and Statistics (AISTATS)*. 2010.
- [6] Michalis K. Titsias and Miguel Lázaro-Gredilla. “Variational Inference for Mahalanobis Distance Metrics in Gaussian Process Regression”. In: *Advances in Neural Information Processing Systems (NeurIPS)*. 2013.